Towards Achieving Circular Economy in the Production of Silica from Rice Husk as a Sustainable Adsorbent

Alba Rodriguez-Otero, Anne Galarneau, Méghane Drané, Frederic Marias, Victor Sebastian, Andrew Wilson, Dav Grégoire, Sadia Radji, Frederic Marias, Jan H Christensen, et al.

processes

MDPI

Article

Towards Achieving Circular Economy in the Production of Silica from Rice Husk as a Sustainable Adsorbent

Alba Rodriguez-Otero [1,2], Anne Galarneau [3], Méghane Drané [4], Vicmary Vargas [1], Victor Sebastian [5,6,7], Andrew Wilson [8], David Grégoire [8], Sadia Radji [1], Frederic Marias [4], Jan H. Christensen [2] and Brice Bouyssiere [1,*]

1 Universite de Pau et des Pays de l'Adour, E2S UPPA, CNRS, IPREM, UMR5254, Technopôle Hélioparc, 2 Avenue du Président Angot, 64053 Pau, France; alba.rodriguez-otero@univ-pau.fr (A.R.-O.); vicmary.vargas@univ-pau.fr (V.V.); sadia.radji@univ-pau.fr (S.R.)
2 Analytical Chemistry Group, Department of Plant and Environmental Sciences, University of Copenhagen, 1871 Frederiksberg, Denmark; jch@plen.ku.dk
3 ICGM, Univ Montpellier, CNRS, ENSCM, 34293 Montpellier, France; anne.galarneau@enscm.fr
4 Laboratoire de Thermique, Energétique et Procèdes-IPRA, University Pau & Pays Adour, EA1932, 64000 Pau, France; mdrane@univ-pau.fr (M.D.); frederic.marias@univ-pau.fr (F.M.)
5 Department of Chemical Engineering and Environmental Technology, Universidad de Zaragoza, Campus Río Ebro-Edificio I+D, 50018 Zaragoza, Spain; victorse@unizar.es
6 Instituto de Nanociencia y Materiales de Aragón (INMA), Universidad de Zaragoza-CSIC, c/María de Luna 3, 50018 Zaragoza, Spain
7 Networking Research Center on Bioengineering Biomaterials and Nanomedicine (CIBER-BBN), 28029 Madrid, Spain
8 Universite de Pau et des Pays de l'Adour, E2S UPPA, CNRS, LFCR, UMR5150, 64600 Anglet, France; andrew.wilson@univ-pau.fr (A.W.); david.gregoire@univ-pau.fr (D.G.)
* Correspondence: brice.bouyssiere@univ-pau.fr

Abstract: The growing concern over water pollution and waste management requires innovative solutions that promote resource efficiency within a circular economy. This study aims to utilize rice husk (RH) as a sustainable feedstock to develop highly porous silica particles and generate valuable by-products, addressing the dual challenges of waste reduction and water contamination. We hypothesize that optimizing the production of amorphous silica from acid-washed RH will enhance its adsorptive properties and facilitate the concurrent generation of bio-oil and syngas. Amorphous silica particles were extracted from acid-washed RH with a yield of 15 wt% using a combination of acid washing at 100 °C, pyrolysis at 500 °C, and calcination at 700 °C with controlled heating at 2 °C/min. The optimized material (RH2-SiO_2), composed of small (60–200 nm) and large (50–200 µm) particles, had a specific surface area of 320 m^2/g, with funnel-shaped pores with diameters from 17 nm to 4 nm and showed a maximum cadmium adsorption capacity of 407 mg Cd/g SiO_2. Additionally, the pyrolysis process yielded CO-rich syngas and bio-oil with an elevated phenolic content, demonstrating a higher bio-oil yield and reduced gas production compared to untreated RH. Some limitations were identified, including the need for bio-oil upgrading, further research into the application of RH2-SiO_2 for wastewater treatment, and the scaling-up of adsorbent production. Despite the challenges, these results contribute to the development of a promising adsorbent for water pollution control while enhancing the value of agricultural waste and moving closer to a circular economy model.

Keywords: rice husk; silica; adsorbent; circular economy

Citation: Rodriguez-Otero, A.; Galarneau, A.; Drané, M.; Vargas, V.; Sebastian, V.; Wilson, A.; Grégoire, D.; Radji, S.; Marias, F.; Christensen, J.H.; et al. Towards Achieving Circular Economy in the Production of Silica from Rice Husk as a Sustainable Adsorbent. *Processes* **2024**, *12*, 2420. https://doi.org/10.3390/pr12112420

Academic Editor: Avelino Núñez-Delgado

Received: 24 September 2024
Revised: 25 October 2024
Accepted: 30 October 2024
Published: 2 November 2024

1. Introduction

The circular economy aims to maximize the efficient use of resources and minimize waste. In alignment with the European Union's 2050 climate neutrality goal, the European Commission proposed a Circular Economy Action Plan, pointing out that, with increasing

global biomass and fossil fuel consumption, annual waste is projected to rise by 70% by 2050 [1]. Agriculture, due to its elevated biomass production is one of the primary areas of interest. Rice, one of the top four global crops, generates significant agricultural waste in the form of rice husk after the milling process. In 2023, the European Union produced approximately 300,000 to 450,000 tons of rice husk [2]. The rice husk (RH) dry composition includes 15–28 wt% silica, with traces (3–13 wt%) of metallic impurities (K_2O, Al_2O_3, CaO, MgO, Fe_2O_3, etc.), and 72–85 wt% lignocellulose (15–22 wt% lignin, 12–29 wt% hemicellulose, and 29–36 wt% cellulose) [3]. Traditionally, RH has been mostly burned for thermal energy, causing air pollution, or used as a filler in construction materials [4]. However, its high silica content has sparked interest in more sustainable applications. Recent European projects like RiceRes have explored recovering silica from RH for biopolymer composites [5]. Industrial applications of RH-derived silica include fuel-saving tires by Pirelli in Brazil and a recent project by Solvay in the tire industry [6,7].

Various methods exist for producing silica from RH, including chemical extraction/precipitation from rice husk ash (RHA) [8–10], the direct calcination of acid-pretreated RH [11–18], the chemical extraction/precipitation/sol–gel method on RHA after pyrolysis [19–22], or calcination after pyrolysis [23,24]. The mesoporous silica materials produced from acid-pretreated RH followed by pyrolysis give the silica materials with the highest surface area either after calcination (350 m^2/g) [23] with silica featuring a broad mesopore size distribution from 4 to 10 nm or after alkali extraction followed by acidic precipitation (370 m^2/g) [19] with silica featuring a narrow pore size distribution of 10 nm.

The alkali extraction of silicate from RHA and precipitation using acids, polymer additives, or co-solvents is a commonly used process due to the ease with which the particle size and porosity can be controlled by modifying synthesis conditions (the concentration of the silica precursor, organic co-solvents, and reaction temperature) [19].

Nonetheless, the advantage of the combined process of pyrolysis and calcination is the reduction in the use of chemicals, the simplicity due to the possibility of using the same infrastructure for both processes (pyrolysis and calcination), and the use of biomass-derived energy.

Pyrolysis is an established tool for a circular economy which has been shown to contribute to an economic and social growth by addressing waste management and energy consumption [25]. Lignin and cellulose are valuable raw materials for producing bio-oil and syngas through pyrolysis. The liquid product of pyrolysis, bio-oil, can replace fossil fuels or be used for producing value-added chemicals. Pyrolysis products from RH have been studied in recent years [21,24]. Bio-oils obtained from fast pyrolysis were obtained with similar compositions to other biomass-derived bio-oils, although upgrading was needed to reduce the high water, solid, and ash content. A comprehensive analysis of RH valorization was conducted by Su et al. (2020) [21], which revealed the CO-rich syngas and phenol-abundant bio-oil (phenols 42.08%) obtention through pyrolysis. Moreover, catalytic pyrolysis, with activated carbon as the catalyst, increased the yield of phenolic compounds (>95%). The resulting amorphous SiO_2 from catalytic pyrolysis obtained through the chemical extraction/precipitation process was not characterized [21]. On the other hand, Gómez-Vásquez et al. (2022) [24] provided a full characterization of the obtained SiO_2 after pyrolysis and the calcination of RH. Showing that without the acid pretreatment of RH and the use of a high calcination temperature, biogenic silica features a low specific surface area (18–27 m^2/g). Acid pretreatment prior to calcination is a crucial step in the production of pure amorphous silica featuring a high specific surface area, as it removes metallic impurities present in RH. In particular, potassium (K) is responsible for promoting the crystallization of silica during calcination, leading to a reduction in surface area [14]. The syngas produced during the pyrolysis of acid-pretreated RH of Gómez-Vásquez et al. (2022) [24] had a high N_2, CO, and CO_2 content, but the bio-oil produced was not characterized.

Studies on RH pyrolysis often have a narrow focus and overlook the functional potential of silica from RH. The RH-SiO_2 mesoporosity, tunable specific surface area,

easiness to functionalize, and thermal and chemical stability make silica from RH, as with silica in general, an interesting material for adsorption for water cleaning [26–29]. As demand grows for low-cost and easily regenerable adsorbents, the research on RH-derived silica functionality as an adsorbent is at an early stage.

Biogenic silica as an adsorbent has been proven to remove both organic and inorganic pollutants from wastewater. RH-SiO_2, covered by silanol groups that are deprotonated at a pH of wastewater ranging from 2 to 8, results in a net negatively charged surface. The concentration of SiO^- groups at the silica surface increases with a pH above the isoelectric point of silica (pH 2). At pH levels typical of wastewater (pH 6–8), RH- SiO_2's silanol groups deprotonate, resulting in a net negatively charged surface that facilitates electrostatic interactions with positively charged compounds. This interaction, alongside porosity diffusion and hydrogen bonding, enhances the adsorption efficiency [30–34].

Electrostatic interactions are crucial for recovering toxic metals—such as cadmium (II)—discharged into the environment from mining, chemical plants, and agriculture. Studies have confirmed that RH-SiO_2 can adsorb these metals effectively, with the subsequent regeneration achieved through chemical regeneration using mineral and organic acids, employing cation exchange mechanisms [24,26,35,36]. While the existing literature reports studies on the application of RH-derived silica for metal adsorption, these studies often disregard the optimization of the extraction process and the characterization of by-products generated during it.

In conclusion, the pyrolysis process of rice husk can be self-sustaining, utilizing energy from the combustion of syngas, bio-oil, and char in other processes while producing valuable compounds. Despite many studies exploring rice husk pyrolysis, most focus primarily on characterizing specific by-products, leaving a notable gap in the simultaneous extraction of silica and utilization of pyrolysis by-products, especially regarding silica's potential as a low-cost adsorbent. Optimizing the extraction process to obtain silica with enhanced porosity could further improve the economic viability of this approach.

This study aims to fill this gap by highlighting the co-production of valuable chemicals and refining the extraction process to yield a highly porous, efficient adsorbent. To achieve this, the pyrolysis by-products were characterized to assess the effect of acid pretreatment on RH, while silica production parameters were optimized to enhance mesoporosity. Additionally, batch tests evaluated the cadmium adsorption using RH-SiO_2, and the cadmium-loaded adsorbent was extensively characterized. This approach aims to enhance the circular economy potential of the process by increasing the value of rice husk waste products.

2. Materials and Methods

2.1. Rice-Husk-Silica Production

The rice husk was obtained from the rice mill Arroz Brazal Arrocera del Pirineo in Zaragoza (Aragon, Spain). An extensive literature review was conducted to identify the optimal parameters for the acid washing step. The results demonstrated that the type of acid, rice-husk-to-acid ratio, and the leaching temperature are key variables in silica production from rice husk (RH) [28]. Hydrochloric acid in a ratio of 1.49 mol HCl/kg RH was employed and HCl pretreatment temperature was explored (Figure 1).

Initially, 50 g of RH were cleaned with tap water five times (500 mL each) to remove impurities. The water cleared up with each washing step, and the final washing was conducted with distilled water. Subsequently, 6.22 mL of HCl (ACS reagent, 37% HCl) (Sigma-Aldrich, St. Louis, MO, USA) were diluted in 750 mL of distilled water to obtain a 0.1 M HCl solution. The acid leaching process was conducted by mixing the 50 g of RH with 750 mL of 0.1 M HCl solution in a rounded balloon. The balloon was either heated with a jacket at 100 °C for 3 h or maintained at 20 °C for 24 h under mechanical stirring with a paddle at 40 rpm. Following acid washing, the RH was washed five times with 500 mL of deionized water until a neutral pH was achieved, after which it was dried overnight in an oven at 80 °C.

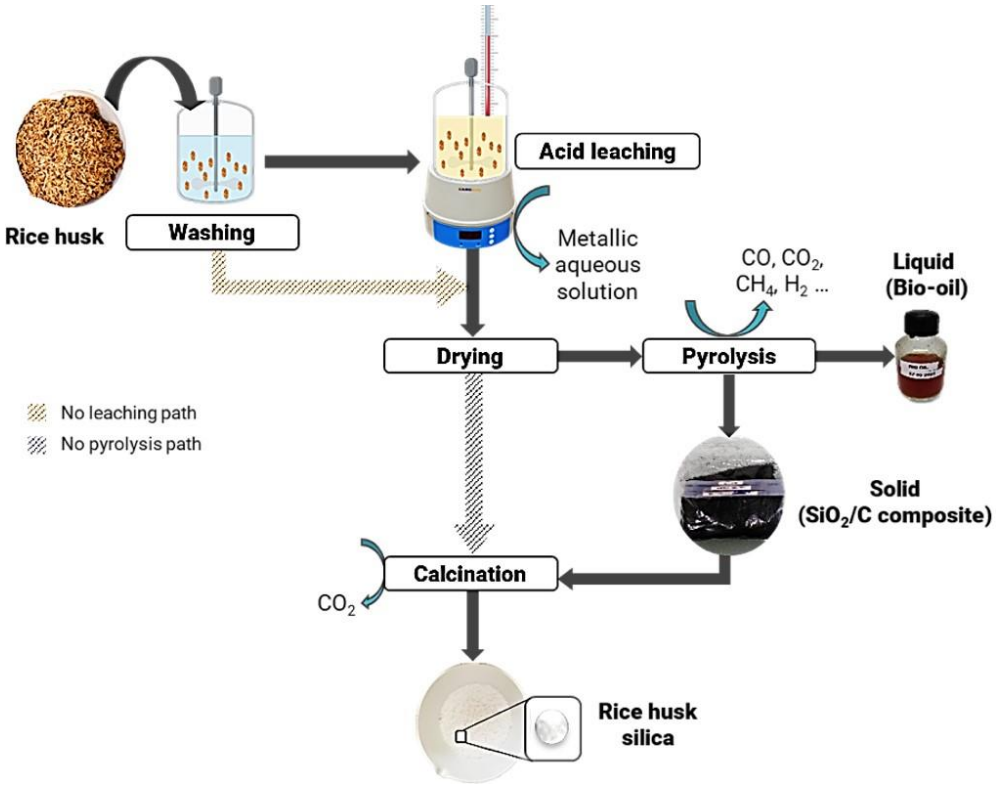

Figure 1. Experimental procedure explored for RH-SiO_2 production from RH.

Once the acid-washed RH (AWRH) had been dried, it was taken to thermal treatment. Then, different RH-SiO_2 samples were produced under different conditions (Table 1) with the objective of achieving mesoporous silica featuring high specific surface area. The samples were subjected to either direct calcination (AWRH3 and AWRH4), or to pyrolysis before calcination (AWRH1, AWRH2, and AWRH5); additionally, the effect of acid pretreatment temperature and calcination slope were evaluated.

Table 1. Thermochemical operational conditions for AWRH-silica production.

RH Samples	Acid Washing Temperature (°C)	Acid Washing Time (h)	Pyrolysis 500 °C 1 h 10 °C/min	Calcination Slope (°C/min)	Calcination Temperature (°C)
AWRH1	100	3	pyrolyzed	10	700 for 3 h
AWRH2	100	3	pyrolyzed	2	700 for 3 h
AWRH3 *	20	24	-	2	700 for 3 h
AWRH4	100	3	-	2	700 for 3 h
AWRH5	20	24	pyrolyzed	2	700 for 3 h

* This sample was hand milled after calcination step.

In Table 1, the fixed parameters include the calcination and pyrolysis temperatures and times. A literature review of pyrolyzed RH revealed a range of pyrolysis temperatures between 500 and 800 °C [28]. We selected the lower end of this range (500 °C) to minimize energy consumption while ensuring complete pyrolysis of the biomass, based on trials indicating that this temperature and duration were sufficient. Similarly, the calcination temperature of 700 °C was chosen from the literature, as studies have shown it to be effective for silica production from rice husks [28]. The time for calcination was determined through trials to ensure complete carbon removal. While further investigation into varying these parameters—especially modifying the pyrolysis temperature to study its effects on

by-products—would have been valuable, time constraints limited our ability to explore these variables.

The objective of the calcination process was to eliminate carbon content of the biomass, thereby obtaining inorganic pure amorphous SiO_2. A sample of 200 g of AWRH was subjected to calcination in a laboratory furnace (Carbolite Gero, Hope Valley, UK, Gero 30–3000 °C) at heating slopes of 10 °C/min or 2 °C/min until the selected temperature (700 °C) was reached, after which the process was maintained for 3 h.

The pyrolysis of RH (200 g) was carried out on a thermobalance (Figure S1) under a nitrogen atmosphere at a constant flow rate of 13.1 g/min with an oxygen concentration inferior to 2 vol% to provide inert conditions. The pyrolysis starting temperature was 30 °C, and then heated at a rate of 10 °C/min to 110 °C and held for 60 min, and then heated at a rate of 10 °C/min to 500 °C and held for 60 min. The pyrolysis conditions were optimized beforehand.

During pyrolysis, three products were obtained: non-condensable gases, bio-oil, and solid char containing silica. Pyrolysis gas was analyzed by μGC (Varian, CA, USA) which was located at the gas outlet of the thermobalance. Bio-oil from AWRH and RH pyrolysis was further characterized by GC-MS.

The effect of RH acid pretreatment was tested with samples from acid washing at 100 °C during 3 h (AWRH) and non-acid-washed samples (RH) followed by pyrolysis 500 °C 1 h and calcination 700 °C 3 h (2 °C/min).

2.2. Rice-Husk-Silica Characterization

Nitrogen adsorption isotherms at 77 K were determined using a gas analyzer Micromeritics TriStar II. All samples were outgassed under vacuum at 350 °C for 3 h prior to analysis. The specific surface area (S_{BET}) and the C_{BET} parameter were determined using the Brunauer–Emmett–Teller (BET) equation following the Rouquerol criteria [37]. The presence of microporosity was evaluated by t-plot analysis. The macropore diameter and volume were determined by mercury intrusion porosimetry performed through an Autopore IV apparatus (Micromeritics, Norcross, GA, USA).

The morphology of the optimized silica from RH, named RH2-SiO_2, obtained from AWRH2, was observed by scanning electron microscopy (SEM, Hitachi S-4700, Hitachi, Tokyo, Japan) and transmission electron microscopy (TEM, Tecnai G2 F30, FEI, The Netherlands, Eindhoven). The column chart of the particle size distribution (PSD) was obtained using the ImageJ software 1.6.0 (LOCI, University of Wisconsin) according to TEM images. Scanning transmission electron microscopy (STEM) images were acquired using a high-angle annular dark field detector (HAADF) in a FEI XFEG TITAN electron microscope (FEI, The Netherlands, Eindhoven) operated at 300 kV. Elemental analysis was carried out with an EDAX detector in scanning mode. Size and morphology were confirmed with atomic force microscopy (AFM), the Multimode-Nasoscope VIII (BRUKER, Billerica, MA, USA) operating under ambient conditions, in the intermittent contact mode. Dynamic light scattering instrument (DDL Zetasizer, Malvern Panalytical, Malvern, Worcestershire, UK) with a particle size range of 1 nm to 10 μm for particle analysis, He-Ne laser (wavelength 633 nm) and a backscatter detection (173°) were used to examine the size distribution of RH2-SiO_2. The sample was dissolved in distilled water (DW) with a concentration of 0.02 g/mL. The solution was ultrasonicated during 15 min, then, we let larger particles sediment for 30 min. The zeta potential was measured in the same device, and SiO_2 particles were equally suspended in ultra-pure water, and solutions at different pH (2–9) were prepared with HNO_3 (0.1M) and NaOH (0.1M) solutions. The results were obtained using the Smoluchowski theory approximation, and each sample was measured 3 times at 25 °C. The manufacturer software (Zetasizer 7.12) was used to assess particle diameter (intensity distribution), the polydispersity index (PDI), and z-potential values. The pH point of zero charge (pH_{PZC}) of RH2-SiO_2 was determined by identifying the point where zeta potential value is equal to zero. Attenuated total reflectance infrared spectroscopy (ATR-FTIR) was used to determine the functional groups present on the surface of the

prepared material (RH2-SiO_2). The ATR-FTIR were acquired using a ThermoScientific Samrt iX Nicolet iS20 infrared spectrometer (ThermoScientific, Waltham, MA, USA). The spectra were obtained from 500 to 4000 cm^{-1} in transmittance mode with a resolution of 4 cm^{-1} after 128 scan accumulations.

2.3. Bio-Oil Characterization by GC-MS Analysis

Identification of the organic phase of bio-oil components was performed by gas chromatography coupled to mass spectrometry (GC-MS). The sample was diluted by a factor of 50% in tetrahydrofuran (THF) as the solvent. GC-MS analysis was performed in gas chromatographer Agilent 8860 GC System (Agilent, Santa Clara, CA, USA) coupled to a mass spectrometer Agilent 5977B GC/MSD using a capillary column HP-5MS UI of 30 m length, 0.250 mm diameter, and 0.25 µm film thickness. In GC-MS analysis, detector temperature was 300 °C, injector temperature 270 °C, and carrier gas (N_2) pressure 2 psi. The initial temperature was set to 70 °C, and then it was heated until 280 °C at a rate of 8 °C/min and held for 5 min. Compounds were identified using Agilent software NIST MS Search 2.0.

2.4. RH2-SiO_2 Application for Adsorption of Cadmium in Batch

The adsorption capacity of RH2-SiO_2 was evaluated in batch experiments conducted in cadmium aqueous solutions. The metallic solutions were made from a 1000 ppm commercial standard solution of metallic cadmium in 5% HNO_3 (Agilent, Santa Clara, CA, USA). The standard solution was diluted to 5–100 ppm concentrations in MilliQ water adjusted to pH 8, with NaOH 0.1 M. A total of 20 mg of the material was placed in contact with 100 mL of the solutions, and the experiments were conducted under magnetic stirring at 700 rpm in 150 mL plastic flasks (20 °C).

Following a 3 h contact period, at equilibrium, each batch was subjected to centrifugation at 6000 rpm for seven minutes. At pH 3–8 and 20 °C, amorphous silica's solubility is considered to be slow; thus, for the duration of the experiment, it is neglected [38]. The supernatant was then sampled for total analysis by inductively coupled plasma mass spectrometry (ICP-MS, Agilent 8000, CA, USA). The adsorption capacities at different initial concentrations of cadmium were quantified by following the remaining cations of cadmium in the aqueous solution after the treatment has been carried out. This was achieved by means of ICP-MS. Each solution was diluted 104 times with MilliQ water and acidified to 2% HNO_3 to a final volume of 5 mL. Argon was used as the carrier gas, with a flow rate of 1.06 L/min. Atomic interferences on Cd were eliminated using helium (3.5 mL·min^{-1}) gas in a collision cell. The collision cell flow rate was helium (3.5 mL/min). The radiofrequency (RF) power was set at 1500 W, the sample chamber (S/C) temperature at 2 °C, and the isotope monitored for cadmium was Cd 112.

The solid recovered from the experiment with an initial concentration of 100 ppm Cd was dried at 80 °C for further surface characterization. This was carried out with transmission electron microscopy (TEM), scanning transmission electron microscopy (STEM) high-angle annular dark-field (HAADF), and energy-dispersive X-ray spectroscopy (EDX) analysis, as well as atomic force microscopy (AFM) analysis.

3. Results and Discussion

3.1. Effects of Acid Washing of Rice Husk on Pyrolysis By-Products

3.1.1. Characterization of Pyrolysis By-Products

The mass fractions of the products obtained from AWRH (water- and acid-washed) and RH (only water-washed) pyrolysis are shown in Figure 2a. The pyrolysis at 500 °C of AWRH yielded a 34 wt% of char containing silica, 42 wt% of bio-oil, and a non-condensable gas fraction of 24 wt%. RH pyrolysis produced a similar char fraction (38 wt%), fewer bio-oil (20 wt%), and higher gas (35 wt%). The presence of solids in the bio-oil produced by RH pyrolysis could indicate that some char particles escaped the solid separation system. This observation could explain the overall yield of products to be lower than 100% for RH,

potentially due to the loss of char. An increase in the yield of bio-oil with acid-pretreated RH has been observed in literature [21,39]. Alkali and alkaline earth metals (AAEMs) are suggested to have catalytic effects on the decomposition of cellulose and hemicellulose, which enhance the decomposition of biomass to lower temperatures while increasing the char and gas yields at the expense of bio-oil [39]. With regard to the gas volumetric fraction for both samples (Figure 2b), CO was predominant, followed by CO_2, H_2, CH_4, and C^{2+} gases. It is noteworthy that the CO_2 fraction decreased for AWRH, while there was an increase in CO. These findings are consistent with those reported by Su et al. (2020) [21] following the demineralization of RH.

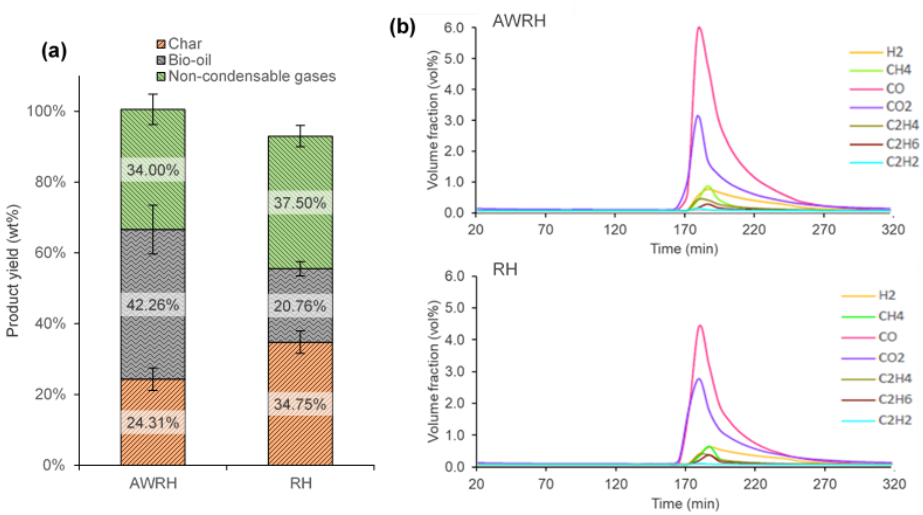

Figure 2. (**a**) Yield on the production of char, bio-oil, and non-condensable gases from pyrolysis of rice husk (RH) and acid-washed RH (AWRH); and (**b**) evolution of volume fraction of non-condensable gas composition during pyrolysis of AWRH and RH.

The organic phase of the bio-oil was subjected to analysis by gas chromatography–mass spectrometry (GC-MS). Figure 3 depicts the primary classes of compounds identified, including acids, aldehydes, phenols (methoxyphenol and alkylphenols), furans, ketones, and monocyclic and polycyclic aromatic compounds for AWRH and RH. The total relative proportion of all these groups was less than 100% due to the presence of unidentified compounds. The relative content of monocyclic aromatic hydrocarbons (alkyl benzene) is notably high for both AWRH and RH, with values of 53 and 72 wt%, respectively. This observation aligns with the findings of Zhang et al. (2018) [40]. The main compounds in this group were benzene, ethylbenzene, and xylene (see Table S1). The amount of alkylbenzene fraction was reduced for acid-pretreated RH (AWRH) in comparison to RH (from 72 to 53%), at the expense of total phenols (methoxyphenols and alkylphenols) (from 17 to 27%). Phenolic compounds are derived from the depolymerization of lignin [41]. AAEMs have been observed to promote the secondary cracking of volatile phenols through a dehydration reaction to form aromatic hydrocarbons [40]. Collectively, these observations suggest that the enrichment of phenols in liquid products coming from the pyrolysis of acid-pretreated RH may indicate the potential for their extraction as valuable chemicals.

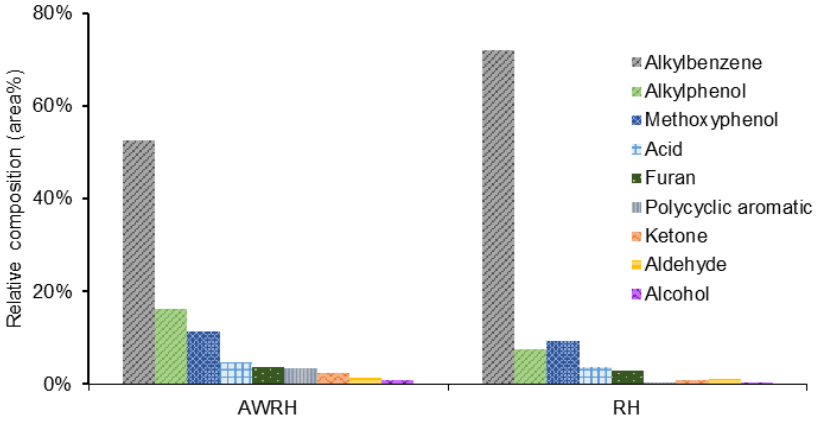

Figure 3. Relative content (area%) of major group components detected in organic phase of bio-oil obtained via pyrolysis of AWRH and RH obtained by GCMS analysis.

3.1.2. Calcination of AWRH and RH Ashes

The calcination at 700 °C for 3 h (2 °C/min) of the ashes obtained from pyrolysis at 500 °C for 1 h resulted in the removal of residual char in the solid to recover silica. After calcination, the RH (not-acid-washed RH) ashes exhibited a pinkish coloration (Figure 4), which can be attributed to the crystallization of SiO_2. This phenomenon can be catalyzed at lower temperatures in the presence of K, which is one of the main inorganic compounds in RH ash [3]. The calcination of AWRH (HCl-pretreated RH, 100 °C, 3 h) ashes resulted in the formation of a silica product with white coloration. The whiteness of silica is directly correlated with the amorphous silica content [23]. The yield of RH-SiO_2 obtained from the calcination of the AWRH2 ashes was 40.7 ± 3.0 wt%, representing a yield of 15.1 ± 3.0 wt% from the original rice husk, while the yield for the not-washed RH ashes was 12.5 ± 0.1 wt%.

Figure 4. Pictures of the effect of acid pretreatment of RH through pyrolysis and calcination processes.

Attenuated total reflectance infrared spectroscopy (ATR-FTIR) was used to determine the functional groups present on the surface of the prepared material from AWRH (RH-2). The ATR-FTIR spectra in the wave region of 4000–500 cm^{-1} are shown in Figure S2. Numerous peaks are detected in RH-SiO_2, similar to those found in commercial amorphous silica. The most intense peak is at 1074 cm^{-1}, followed by one at 813 cm^{-1}, which are

assigned to Si–O symmetrical and asymmetrical groups. The peaks from 2400 cm^{-1} to 2000 cm^{-1} correspond to the elongation vibrations of O=C=O from the atmospheric CO_2 adsorption, or carbon impurities from the calcined rice husk [20].

3.2. Textural Characteristics of Silica Materials from RH

The RH(1,2,3,4,5)-SiO_2 produced from acid-treated RH (AWRH1,2,3,4,5) following the five different protocols listed in Table 1 were analyzed by nitrogen adsorption at 77K (Figure 5). The shapes of the isotherms were all the same and were of the type IV characteristics of mesoporous materials featuring a large pore size distribution between 4 and 17 nm, which results the spaces in between the nanoparticles. We can propose that these silica materials featured "funnel-shaped" pores with a 17 nm larger size decreasing to 4 nm, corresponding to an average of 6.5 nm. This kind of hysteresis is found for mesopores with the depth shorter than the pore diameter [42]. To control if the materials also exhibit micropores, the t-plot curves [37] were drawn from nitrogen adsorption isotherms (Figure S3). The evolution of the t-curves is linear at low t, with a straight line going through the origin. This shows that silica from RH possess no micropores. The slope of this straight line at low t allows us to calculate the total surface areas of the materials, which are in good agreement with the BET specific surface areas (S_{BET}) calculated directly from the nitrogen adsorption isotherms. The S_{BET}-specific surface areas of RH-SiO_2 were calculated accurately according to the Rouquerol criteria [37] for three different batches of each of the five protocols (Tables 2 and 3). The average values of S_{BET} were 276, 317, 247, 249, and 188 m^2/g for RH1-SiO_2, RH2-SiO_2, RH3-SiO_2, RH4-SiO_2, and RH5-SiO_2, respectively.

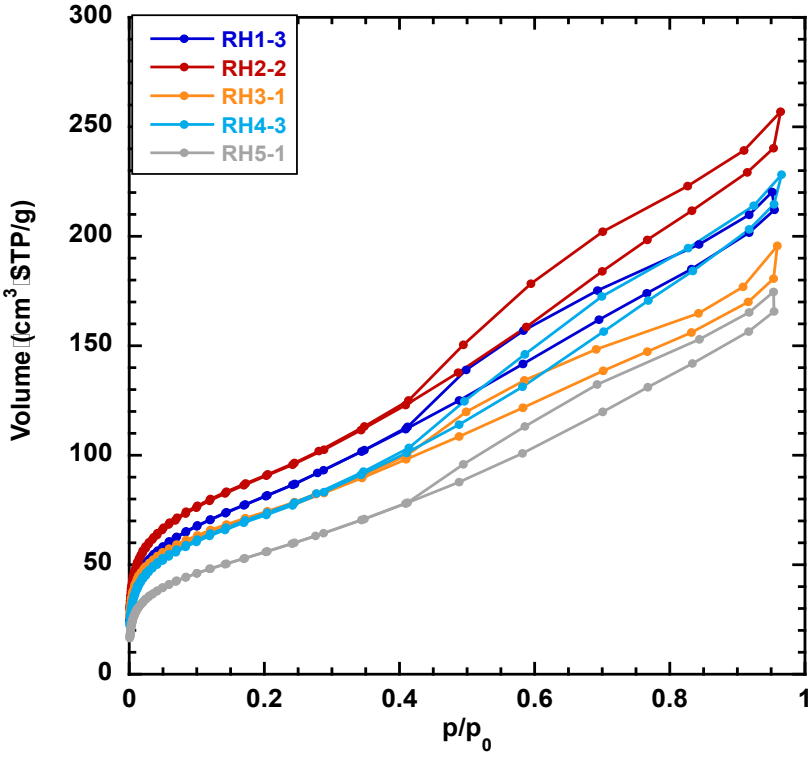

Figure 5. Nitrogen adsorption/desorption isotherms at 77K of some RHx-SiO_2-y obtained from acid-treated RH AWRHx, with x corresponding to the protocol (1 to 5) and y to the batch (1 to 3): (dark blue) AWRH1 giving RH1-SiO_2-3, (red) AWRH2 giving RH2-SiO_2-2, (orange) AWRH3 giving RH3-SiO_2-1, (light blue) AWRH4 giving RH4-SiO_2-3, and (grey) AWRH5 giving RH5-SiO_2-1.

Table 2. Textural characteristics of the silica materials from RH.

SiO_2	BET p/p_0 Domain [a]	S_{BET} m^2/g	C_{BET}	V_{mes} [b] mL/g	$D_{mes\ average}$ nm
RH2-SiO_2-2	$0.049 < p/p_0 < 0.15$	329	91	0.35	6.5
RH4-SiO_2-2	$0.058 < p/p_0 < 0.34$	233	68	0.27	6.5
RH4-SiO_2-3	$0.049 < p/p_0 < 0.34$	266	76	0.31	6.5
RH5-SiO_2-1	$0.083 < p/p_0 < 0.34$	208	58	0.24	6.5
RH5-SiO_2-2	$0.142 < p/p_0 < 0.34$	190	49	0.22	6.5
RH5-SiO_2-3	$0.169 < p/p_0 < 0.34$	188	61	0.22	6.5

[a] in agreement with Rouquerol criteria; [b] taken at $p/p_0 = 0.9$.

Table 3. Summary of results of RH-SiO_2 obtained from 3 batches of each AWRHx, comparison with silica produced from raw RH without acid pretreatment.

Silica	HCl 0.1M	Duration	Pyr/Calc	$S_{BET\text{-}average}$ m^2/g	S_{BET} Range m^2/g
RH1-SiO_2	100 °C	3 h	Pyr [1] (10 °C/min)	276	213–298
RH2-SiO_2	100 °C	3 h	Pyr [1] (2 °C/min)	317	304–325
RH3-SiO_2	20 °C	24 h	Calc (2 °C/min)	247	228–261
RH4-SiO_2	100 °C	3 h	Calc (2 °C/min)	249	232–266
RH5-SiO_2	20 °C	24 h	Pyr [1] (2 °C/min)	188	186–207

[1] Pyr: Pyrolysis at 500 °C for 1 h + Calcination 700 °C for 3 h.

The S_{BET} values revealed important information: the acid treatment of RH at high temperatures (100 °C) and with calcination at a slow rate (2 °C/min) increased the specific surface area of the resulting silica, caused by a larger separation of the nanoparticles in the aggregates. Additionally, pyrolysis at 500 °C before the calcination at 700 °C also had a positive effect on the specific surface area (Table 3). The maximum specific surface area of RH-SiO_2 results from protocol 2, AWRH2 with an acid treatment at 100 °C for 3 h, pre-pyrolysis at 500 °C for 1 h, and calcination at 700 °C for 3 h at 2 °C/min. In the three batches of AWRH2, the highest specific surface area of the resulting silica, named RH2-SiO_2-2, was S_{BET} = 329 m^2/g, with the highest mesopore volume of 0.35 mL/g (Table 3). The obtained silica material had a high surface area, very similar to the one obtained by Gu et al. (2013) through pyrolysis (350 m^2/g) under an N_2 atmosphere at 300 °C [23].

To further characterize the porosity of silica from RH, mercury porosimetry was performed. Surprisingly, the mesopores observed by nitrogen adsorption were not identified by mercury intrusion porosimetry (Figure 6). No pores smaller than 1 µm were detected. This indicates that the mesopores in the silica of RH are not deep enough to be filled by mercury intrusion and are assimilated to a surface rugosity. Mercury porosimetry revealed, however, the presence of macropores with a large pore size distribution and high macropore volume of 3.5 mL/g. This macroporosity is certainly due to interparticle porosity. For RH1-SiO_2 and RH2-SiO_2, obtained without milling, the average macropore is 23 µm, meaning that the majority of the particles have a diameter of 70 µm if a factor 3 is applied between the pore size and pore diameter. After milling, as with RH3-SiO_2 with hand milling, the particle size changes and two distributions of pore size are revealed: one observed at 42 µm (corresponding to interstices between particles with a size of 120 µm) and 200 nm (corresponding to interstices between particles with a size of 600 nm) (Figure S4).

The SEM pictures confirm a broad distribution of particle size of acid-treated RH with particles of 100–200 µm, particles of 50 µm, and some of 5–30 µm (Figure 7). SEM pictures reveal also the presence of pores of 0.9–1.7 µm size on some particles and some smaller pores of 40–60 nm.

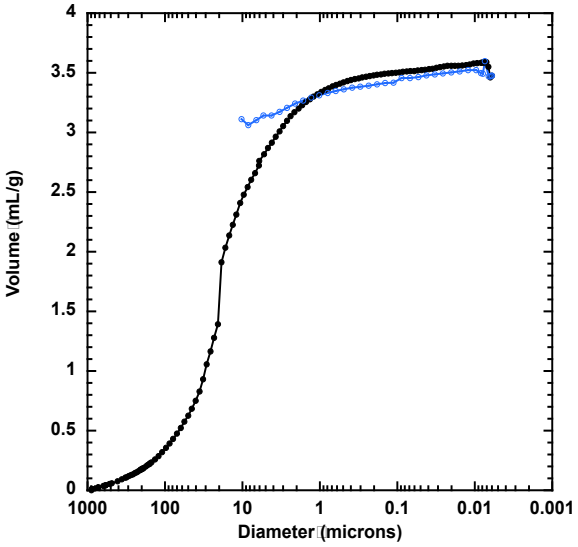

Figure 6. Intrusion (black) and extrusion (blue) curves obtained by mercury porosimetry for the silica material featuring the highest specific surface area: RH2-SiO_2-2.

Figure 7. SEM pictures of acid-treated SiO_2 from RH.

The silica featuring the highest surface area (RH2-SiO_2) is further analyzed by TEM. TEM images show that the large particles of silica from RH are composed of an aggregation of silica nanoparticles (Figure 8a) and also of a mesoporous phase (Figure 8b).

With pore sizes ranging from 4 to 12 nm, with an average of 7.2 ± 2.8 nm in accordance with the result of the mesopore size distribution found by the nitrogen adsorption isotherm with an average of 6.5 nm (Table 2). The nanoparticles appear as regular spheres (Figure 8a), with the mean particle size calculated with image processing software (Image 2.0 J) of 62.4 ± 17.2 nm. The RH2-SiO_2 particle size distribution analyzed by DLS (Figure 9a) with particles diluted in water shows a multimodal distribution with sizes ranging from 50 nm to particles larger than 1 µm. Two main peaks are observed with a maximum at 183 nm and 1 µm. Few particles were observed at 60 nm. Larger sizes are also due to the fact that the hydrodynamic size measured by the DLS is the size of the hypothetical hard sphere that diffuses similarly to the particles being measured [43]. Hence, the diameter calculated is only indicative of the apparent size of the dynamic hydrated particles. It does not signify the actual size of the monodispersed RH2-SiO_2. Therefore, the reported hydrodynamic diameter cannot be used as an approximation of the size but rather for comparison.

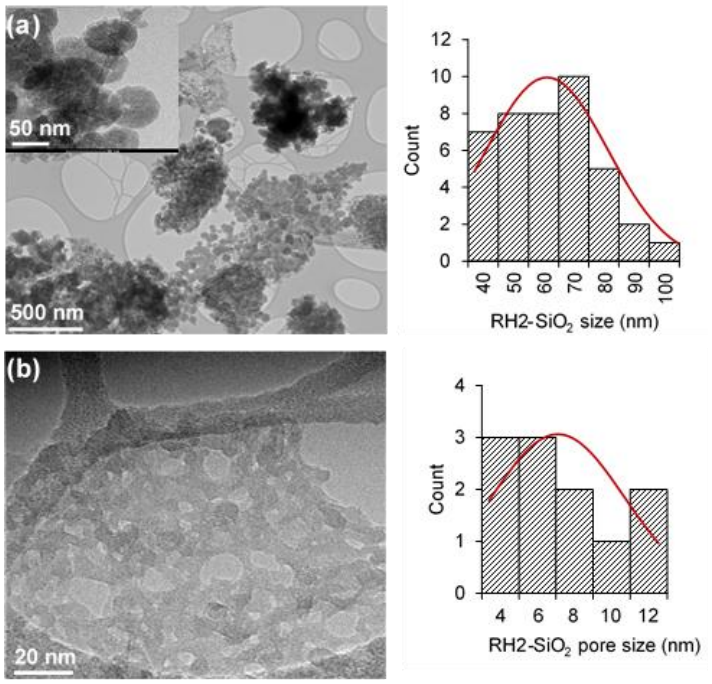

Figure 8. (**left**) TEM images of silica nanoparticles of (**a**) RH2-SiO_2 (**b**) and of the mesoporous phase of RH2-SiO_2. (**right**) (**a**) Particle and (**b**) pore size distribution calculated with Image J software.

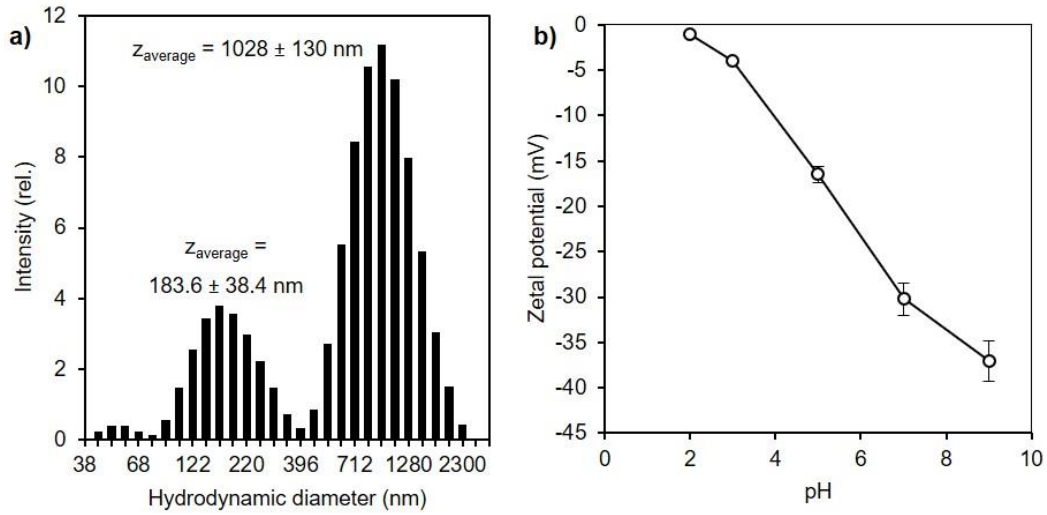

Figure 9. (**a**) Dynamic light scattering (DLS), and intensity size distribution of RH2-SiO_2 as a function of z-average hydrodynamic diameter of RH2-SiO_2, and (**b**) zeta potential measurements performed at different pHs for RH2-SiO_2.

Gu et al. (2013) [23] observed that, with the increase in pyrolysis temperature, larger nanoparticles were obtained under an N_2 atmosphere; in addition, the shape of the particles was affected when increasing the temperature, obtaining spherical particles of 5–8 nm with 500 °C pyrolysis. These particles are smaller than the ones observed in this study. The RH-SiO_2 nanoparticles tend to agglomerate because of inter-particle adhesion forces. The average size corresponds to aggregates, which can be confirmed by the zeta potential values in Figure 9b being lower than ±30 mV at a distilled water pH (~6) [44]. The point of zero charge was determined when the zero potential was equal to zero, pH_{pzc} 2, which aligns with values observed for silica extracted from RH [26]. Above the pH_{pzc} of silica, the RH2-SiO_2 surface is negatively charged, and the charge increases with the increase in pH

to 8, which is a very important character for the further adsorption of positively charged metals in the water depollution process (Figure 9b).

The HAADF-STEM imaging abd-energy-dispersive X-ray spectroscopy (EDX) measurements allowed us to identify the elements present in the RH2-SiO_2 sample in three different points. The elemental composition analysis showed areas with more silicon than others, as in Figure 10, where brighter areas correspond to heavier atoms. This is because the intensity of the scattered electrons detected in HAADF-STEM is proportional to the atomic number of the elements in the sample. Heavier atoms, with higher atomic numbers, scatter electrons more strongly, resulting in brighter spots in the image. Two main peaks corresponding to silicon and oxygen were observed; another small peak corresponding to Ni and K was observed but neglected since it comes from the plating used for the analysis. No other peak was found in the EDX which denotes that the silica observed is pure. The elemental analysis composition performed by EDX and the results are shown in Table 4.

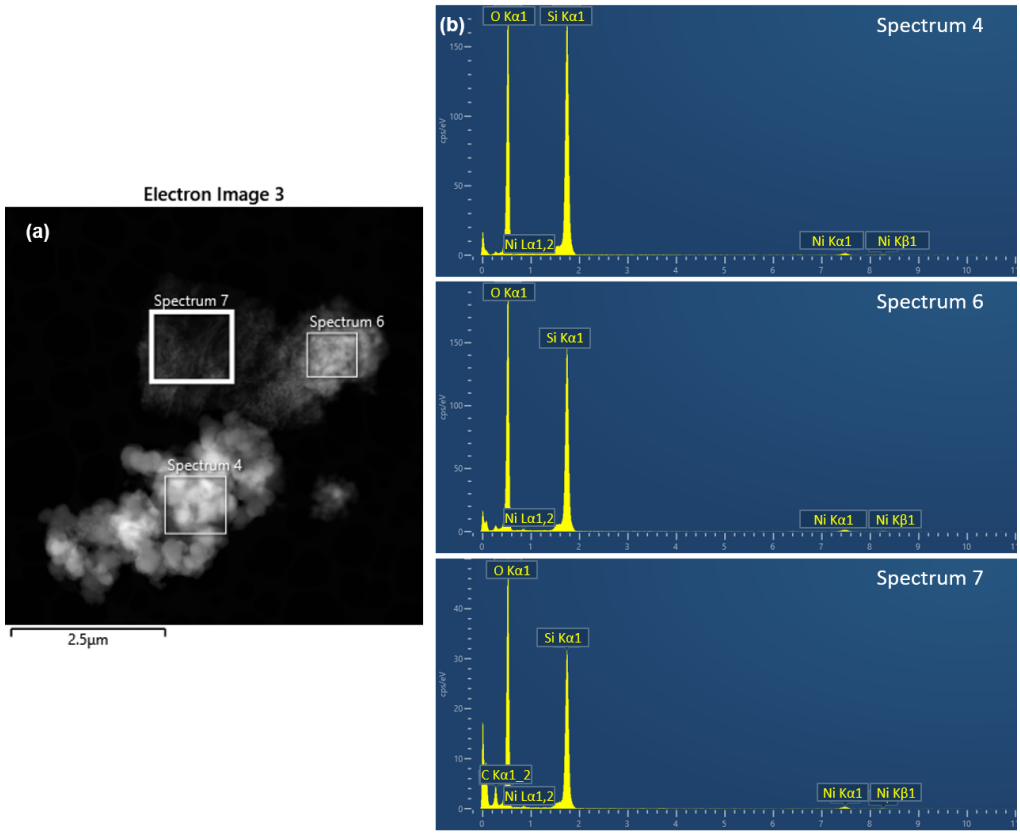

Figure 10. (**a**) STEM-HDAAF-energy-dispersive X-ray spectroscopy (EDX) image of RH2-SiO_2 with the three measured points: (spectra 4, 6, and 7) and (**b**) EDX spectra with elemental identification (Si, O, and Ni) for spectra 4, 6, and 7.

Table 4. Elemental composition of RH2-SiO_2 obtained from EDX analysis of 3 selected sites. Percentages have been corrected removing Ni percentage which comes from the coating.

Elements	**Wt. % Spectrum 4**	**σ**	**Wt. % Spectrum 6**	**σ**	**Wt. % Spectrum 7**	**σ**	**Wt. % Average**	**σ**
O K	50.76%	0.3	56.91%	0.3	60.26%	0.3	**55.98%**	**0.5**
Si K	49.24%	0.3	43.09%	0.3	39.74%	0.3	**44.02%**	**0.5**
Total	100.00%		100.00%		100.00%		**100.00%**	

The weight percentages obtained from the EDX study showed an equivalence in Si:O for different sites of the sample, with an average of 44 wt% Si and 56 wt% O, and

corresponding to an atomic % of Si:O = 1:2.3. An excess of oxygen in relation to the stoichiometric ratio Si:O = 1:2 could be attributed to the presence of water and silanol groups [45]. RH2-SiO_2 has a higher composition in oxygen compared to the results obtained by other researchers of the acid-washed RHA composition Si:O = 1:1.9 at% [46].

Functional groups such as deprotonated silanol present in RH-SiO_2 and its porous structure with a large specific surface area are favorable for the adsorption of metal cations; therefore, Cd^{2+} uptake tests were conducted.

RH2-SiO_2 Adsorption of Metals in Aqueous Solution

The adsorption capacity of the Cd^{2+} solution by RH2-SiO_2 in MilliQ water at pH 8 was tested. At equilibrium, the maximum adsorption capacity was 407.1 ± 0.1 mg Cd/g SiO_2 (Figure 11), which was a high value compared to other experiments in the literature (Table 5). At basic pHs, RH2-SiO_2 was negatively charged due to the deprotonation of silanol groups (pH_{pzc} 2). At pHs higher than the pH_{pzc}, the electrostatic interactions between the cation ion and opposing charge sites in RH-SiO_2 intensifies, favoring metal sequestration [36].

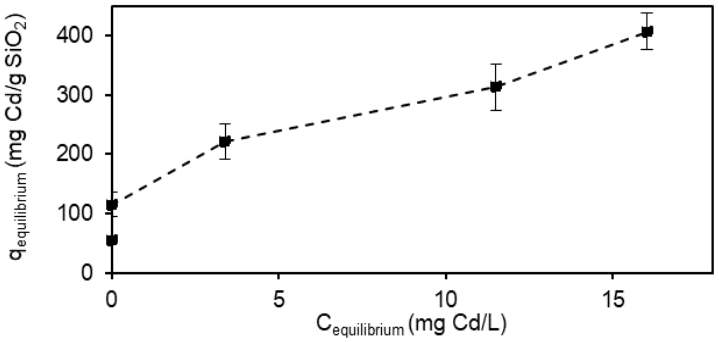

Figure 11. Adsorption capacity (q) of Cd by RH2-SiO_2 at different equilibrium concentrations. Equilibrium time was 3 h, concentration of silica 0.2 g/L. Initial concentrations of Cd in MQ water from 0 to 100 ppm. Quantification made by ICP-MS.

In order to further understand how cadmium is distributed on silica's surface, microscopic analysis techniques were used on the sample of RH2-SiO_2 after being in contact with the 100 pm solution of Cd. Microscopy revealed more agglomerated silica particles compared to the silica before Cd adsorption; the agglomerates had irregular shapes and diameters higher than 1 µm, which seem to be covered by Cd (Figure 12a). Similar morphology changes were observed by Lal et al. (2022) [47] after doping the TiO_2 with neodymium. Some crystallized $Cd(OH)_2$ (identified by elemental analysis and detailed in Figure S5) was found due to the precipitation of Cd in basic media (pH 8) (Figure 12b).

The EDX analysis showed a high ionic adsorption of Cd onto RH2-SiO_2. While Cd was heterogeneously adsorbed among all the samples, Cd was distributed homogeneously on the RH2-SiO_2 surface in specific sites observed in Figure 13. The elemental analysis composition performed by EDX and the results are shown in detail in Table S2. A high concentration of Cd (71 wt.%) was seen in Site 2, followed by oxygen, and then silicon had a smaller presence. As well, in Sites 3 and 5, the composition of Cd was higher than the one of silicon (28 wt.% and 80 wt.%). However, in Site 4, almost no Cd was present in the sample. Lal et al. (2022) [47] observed a 3 wt.% of neodymium on the doped TiO_2 NPs; their observations were over a whole NP, while, in our study, we have focused on specific sites.

While the EDX mapping revealed a heterogeneous distribution of Cd over RH2-SiO_2 (Figure 13), AFM provided deeper insights into the adsorption mechanism. The AFM analysis was carried out with Multimode-Nanoscope VIII(BRUKER) operating in the intermittent contact mode, to examine topographic images of RH2-SiO_2 and RH2-SiO_2-Cd NPs. These NPs were dispersed onto silicon substrates, which were previously cleaned

and treated by UV-ozone to remove any organic contaminant. A rectangular cantilever (Nanosensors NCL-W) was used for imaging, with a free resonance frequency of 15,606 KHz and spring constant of 40 N/m. Both particles analyzed exhibited a similar diameter of around 200 nm. The AFM analysis revealed highly heterogeneous adsorption between different sites. The 2D image displays the height variation as color intensity (Figure S6a,b), with greater differences in intensity observed for RH2-SiO_2 due to the presence of empty pores.

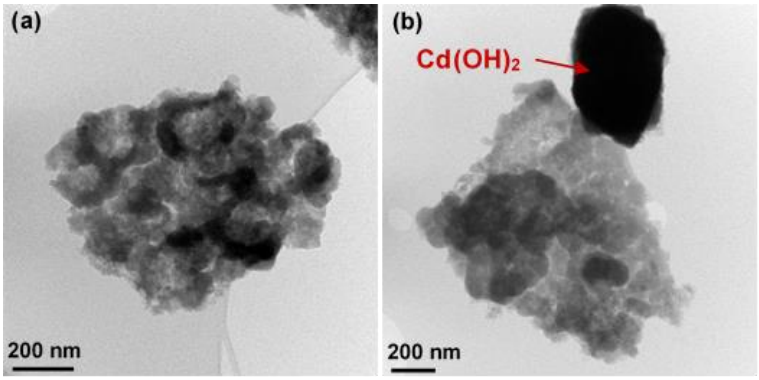

Figure 12. TEM images of agglomerate silica particles of (**a**) RH2-SiO_2 after Cd adsorption and (**b**) RH2-SiO_2 with crystallized $Cd(OH)_2$.

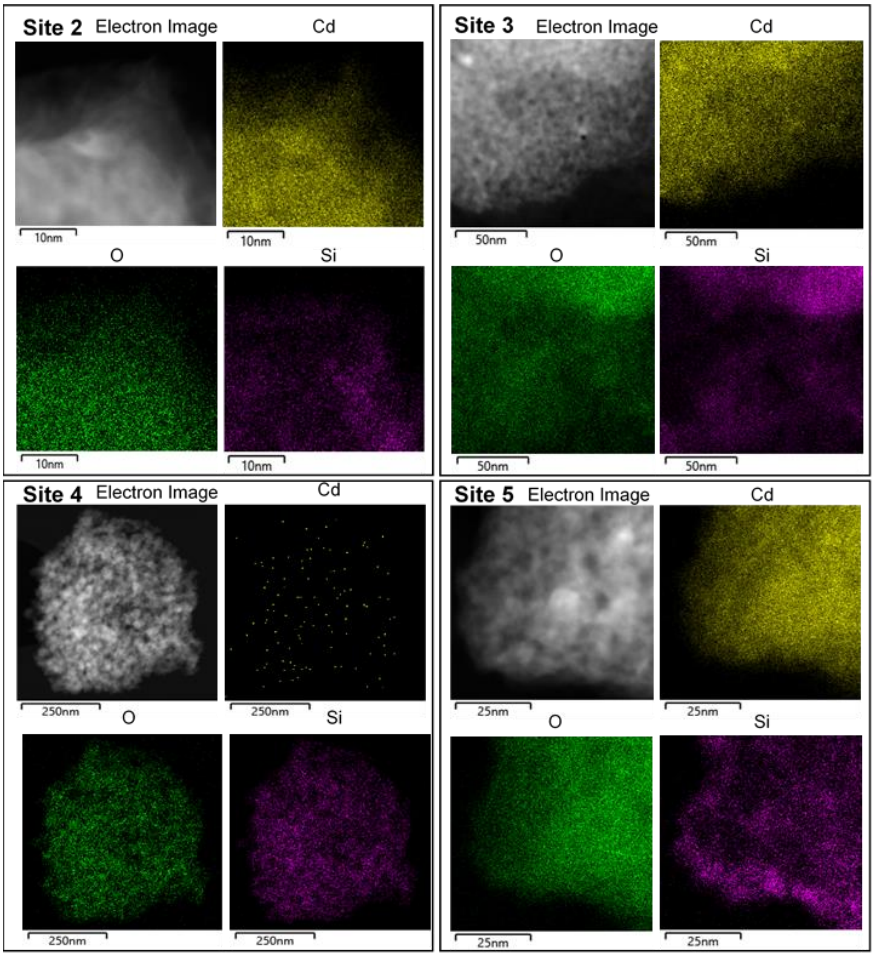

Figure 13. EDX mapping of RH2-SiO_2 particles with Cd on Site 2 (**upper left**), Site 3 (**upper right**), Site 4 (**lower left**), and Site 5 (**lower right**). EDX map color: Cd, yellow; O, green; Si, purple.

AFM imaging allowed us to observe that Cd fills the pores and forms layers on the surface of the RH-silica (Figure S6c; section image). This observation aligns with the findings of Al-Saida et al. (2022) [48], who reported the multilayer adsorption of Cd^{2+} onto nanosilica, suggesting that the adsorption process is primarily driven by differences in the electrostatic charge. The key takeaway is that AFM revealed a smooth profile in the case of RH2-SiO_2-Cd NPs and a rough profile for the pure RH2-SiO_2 NPs, due to the modification of the surface. The combination of EDX and AFM thus offers a more comprehensive understanding of the spatial distribution and the nature of the adsorption process. Nonetheless, further analysis is required to clarify the adsorption mechanism, as ATR-FTIR did not accurately detect the silanol groups, while the transmittance FTIR has proven effective in identifying the functional groups involved in ion sequestration [36,47].

Table 5. Comparison with adsorption of cadmium in metal solutions at 20–25 °C in batch in synthetic water by different adsorbents [1].

Adsorbent	S_{BET} (m^2/g)	pH	qe (mg/g)	te (min)	C_0 (mg/L) Metal	Dosage (g/L)	Author
Nanosilica	307	6	72.1	(72 h)	200	2	[48]
SBA-15	964	6.6	5.6	120	3025	10	[49]
SBA-GSH	187	6.6	112.3	120	3025	10	
PT@MSBA	390	8	34.7	15	3.36	0.13	[50]
MCM-41	1174	5	20.9	120	100	2	[51]
NH_2-50-magMCM-41	571	5	493.2		150	0.1	
Commercial Resin MPX-310	-	3	48.8	720	100	1	[52]
Commercial Resin MPX-317	-	3	106.4	720	100	1	
Commercial Resin TP-214	-	3	116.3	720	100	1	
pPEI-MCF	270	5	625	-	400	-	[53]
MCCR-350	16	5.5	821	720	200	0.2	[54]
RH2-SiO_2	329	8	407.1	180	100	0.2	This work

[1] SBA: Santa Barbara Amorphous, GSH: glutathione grafted, PT@MSBA: polythionine grafted on magnetic SBA, pPEI-MCF: polyethylenimine-functionalized mesocellular silica foam, MCCR: magnetic calcium carbonate nanoadsorbents.

Comparatively, other silica-based materials such as SBA-15, SBA-GSH, PT@MSBA, MCM-41, and nanosilica have shown similar adsorption behavior in batch systems, particularly at pH levels between 5 and 8 [48–51,53]. For instance, microporous nanosilica was obtained using the sol–gel method with TEOS as the precursor; the interaction with Cd^{2+} was studied through molecular dynamics and adsorption isotherms, which determined that it was dominated by electrostatic forces, forming a multilayer uptake [48]. Similarly, mesoporous SBA-15 modified with GSH had a pH_{pzc} of 3.5; while raw SBA-15 exhibited low adsorption, the addition of thiol groups significantly increased its capacity, with the FTIR spectra indicating that Cd interacts mainly with thiol and carboxylic groups more than with silanol groups [49].

Magnetic grafted materials, such as PT@MSBA and NH_2-50-magMCM-41, offer a practical advantage in water treatment applications, as they can easily be recovered from aqueous solutions using magnets [50,51]. MCM-41, derived from acid-leached and calcinated rice husk at 600 °C, was the only rice-husk-based silica material studied for Cd^{2+} adsorption in batch systems found in the literature. Despite its high specific surface area (S_{BET} > 1000 m^2/g), the best results were obtained when MCM-41 was functionalized

with NH_2 groups, even though this reduced by half S_{BET}. Here, ion exchange and surface complexation likely dominated the adsorption process [51].

Additionally, pPEI-MCF, synthesized from TEOS and functionalized with PEI, exhibited chemisorption through a complex formation between amine groups and Cd^{2+} cations. Regeneration was feasible with most of the silica-based adsorbents, which suggests that regeneration will be successful with RH2-SiO_2 [48–51,53]. However, other adsorbents, such as commercial resins or MCCR-350, demonstrated high removal rates, but reusability was not explored [52,54].

While some of these adsorbents address environmental concerns through their regenerability, many are synthesized from non-renewable sources, with few exceptions [50]. In this study, we have demonstrated the production of a highly effective adsorbent derived from renewable resources, which can compete with synthetic alternatives. Additionally, its production via pyrolysis generates valuable by-products, contributing to a more sustainable process. However, as highlighted by Andooz et al. (2023) [55], the current high costs of pyrolysis present a challenge. To make pyrolysis more economically viable, support from public and private institutions is needed to enhance the marketability of its products.

4. Conclusions and Future Recommendations

In the present study, amorphous silica particles RH2-SiO_2, with a high surface area of 317 m^2/g and pore diameters ranging from 17 nm to 4 nm, were extracted from rice husk, achieving a yield of 15.06 $\pm$ 3% after pyrolysis and calcination under optimized conditions. The optimal production method for highly porous silica involved the acid washing of rice husk at 100 °C, followed by pyrolysis at 700 °C and slow calcination at 500 °C with a slope of 2 °C/min. Acid washing also had an effect on pyrolysis by-products as hypothesized. This process yielded a CO-rich syngas and a bio-oil comprising monocyclic aromatics and phenolic compounds, which could prove valuable in the production of relevant chemicals.

Characterization studies revealed that RH2-SiO_2 nanoparticles exhibited a heterogeneous size distribution, ranging from 60 nm to 200 nm, with a tendency to form agglomerates. The negative zeta potential of RH2-SiO_2 at wastewater pH levels (pH_{pzc} 2) facilitated strong electrostatic interactions with cationic compounds, as evidenced by the high cadmium adsorption capacity, which was found to be 407.1 $\pm$ 0.1 mg Cd/g SiO_2. Microscopic analyses showed that cadmium is adsorbed within the pores of the silica and forms multilayers over the surface. Nonetheless, as the ATR-FTIR analysis failed to detect the presence of silanol groups, the conducting of a transmittance FTIR analysis on RH2-SiO_2 pellets is recommended, to confirm the functional groups involved in cadmium sequestration. Additionally, the initial thermodynamic and kinetic tests should be conducted to thoroughly evaluate the adsorption capacity of RH2-SiO_2. Following this, experiments using real water matrices containing competing ions should be performed to assess the ion competition and the long-term functionality of the adsorbent.

This methodology represents a significant step forward in producing highly porous silica-based adsorbents, while simultaneously generating other valuable by-products such as bio-oil and syngas. To further upgrade the bio-oil quality, future work should focus on optimizing pyrolysis conditions, including the introduction of catalysts and the in-depth analysis of the temperature and time parameters. It should be evaluated if the modifications in the pyrolysis protocol would impact the RH2-SiO_2 porosity.

To sum up, this methodology aligns with the EU's circular economy goals for 2050 by promoting resource efficiency and waste reduction. By converting RH—an agricultural by-product that is often incinerated or left to decompose, contributing to greenhouse gas emissions—into valuable products like bio-oil, syngas, excess heat, and silica-based adsorbents, it supports a more sustainable use of resources. The regeneration and reuse of the adsorbent, particularly through cation exchange, could further extend its lifecycle, reducing the need for new materials in the recovery of metals from industrial effluents. Additionally, the potential use of metal-doped RH2-SiO_2 as a catalyst offers opportunities for cleaner industrial processes.

The prospect of scaling up the production of rice-husk-silica-based adsorbents requires the consideration of several key factors. First, the handling of powdered adsorbents can be impractical for large-scale industrial applications; therefore, research should prioritize pelletizing RH-SiO_2 while minimizing any loss in adsorption capacity. Additionally, conducting a comprehensive life cycle analysis of the entire process is recommended. This analysis should address the global warming potential associated with CO_2 emissions during the calcination step if not captured, and evaluate alternative silica extraction methods from rice husk ash (RHA), such as precipitation, which may involve chemicals and energy consumption.

Furthermore, establishing a market for pyrolysis by-products and seeking government incentives for pyrolysis plant development can also foster sustainability, particularly in developing countries that are major rice producers. This approach not only reduces the pressure on non-renewable resources but also opens a path for low-cost water treatment solutions through the produced adsorbents.

Supplementary Materials: The following supporting information can be downloaded at: https://www.mdpi.com/article/10.3390/pr12112420/s1, Figure S1: Scheme of the thermobalance used for pyrolysis, created by the Laboratoire Thermique Energétique et Procédés de l'Université de Pau et des Pays de l'Adour (LaTEP, UPPA); Figure S2: Infrared spectra of RH2-SiO_2 (from AWRH2) and commercial amorphous silica measured by FTIR-ATR; Figure S3: RH2-SiO_2-2 (left) nitrogen adsorption/desorption isotherm at 77K and (right) its t-plot curve. Figure S4: Pore size distributions characterized by mercury intrusion porosimetry for (a) RH1-SiO_2, (b) RH2-SiO_2, and (c) RH3-SiO_2; Figure S5: STEM-HAADF images of RH2-SiO_2 particles and Cd crystals attached onto the silica and the respective EDX spectra of both sites; Figure S6: AFM images obtained by tapping method in 3D of (a1) RH2-SiO_2 before adsorption and (a2) RH2-SiO_2-Cd, in 2D of (b1) RH2-SiO_2 before adsorption and (b2) RH2-SiO_2-Cd, and phase image and section image of (c1) RH2-SiO_2 before adsorption and (c2) RH2-SiO_2-Cd; Table S1: Assigned compounds by GC-MS analysis of the bio-oil sample from AWRH and RH; Table S2: Elemental composition of RH2-SiO_2-Cd obtained from EDX analysis of 4 selected sites. Percentages have been corrected, removing Ni percentage, which comes from the coating.

Author Contributions: Conceptualization, A.R.-O., A.G., V.V. and B.B.; microscopy analysis, V.S.; AFM analysis, S.R.; pyrolysis, M.D. and F.M.; porosity analysis, A.R.-O., A.W. and D.G.; data curation, A.R.-O. and A.G.; writing—original draft preparation, A.R.-O.; writing—review and editing, A.R.-O., A.G., V.S., S.R. and B.B.; supervision, B.B. and J.H.C. All authors have read and agreed to the published version of the manuscript.

Funding: This research received no external funding.

Data Availability Statement: The data presented in this study are available on request from the corresponding author.

Acknowledgments: This project has received funding from the European Union's Horizon 2020 research and innovation programme under the Marie Skłodowska-Curie grant agreement No 945416. V. Sebastian acknowledges the financial support by the Spanish Ministry of Science and Innovation (grant number PID2021-127847OB-I00) and the access to the "Advanced Microscopy Laboratory" ELECMI-LMA and NANBIOSIS ICTSs. CIBER-BBN is an initiative funded by the VI National R&D&i Plan 2008–2011, Iniciativa Ingenio 2010, Consolider Program, CIBER Actions and financed by the Instituto de Salud Carlos III (Spain) with assistance from the European Regional Development Fund. Development Fund. D. Grégoire acknowledges the financial support of the Investissement d'Avenir French programme (ANR-16-IDEX-0002) under the framework of the E2S UPPA hub Newpores.

Conflicts of Interest: The authors declare no conflicts of interest.

References

1. European Commission. Communication from the Commission to the European Parliament, the Council, the European Economic and Social Committee and the Committee of the Regions. A New Circular Economy Action Plan For a Cleaner and More Competitive Europe COM/2020/98 Final. Available online: https://eur-lex.europa.eu/legal-content/EN/TXT/?qid=1583933814386&uri=COM:2020:98:FIN (accessed on 27 June 2024).

2. European Commission. Agriculture and Rural Development. *Agri-Food Data Portal. Rice Production.* Available online: https://agridata.ec.europa.eu/extensions/DashboardRice/RiceProduction.html (accessed on 27 June 2024).
3. Chen, H.; Wang, W.; Martin, J.C.; Oliphant, A.J.; Doerr, P.A.; Xu, J.F.; DeBorn, K.M.; Chen, C.; Sun, L. Extraction of Lignocellulose and Synthesis of Porous Silica Nanoparticles from Rice Husks: A Comprehensive Utilization of Rice Husk Biomass. *ACS Sustain. Chem. Eng.* **2013**, *1*, 254–259. [CrossRef]
4. Mahdi, S.N.; Babu RD, V.; Shivakumar, M.; Abdullah, M.M.A.B. Mitigation of environmental problems using brick kiln rice husk ash in geopolymer composites for sustainable development. *Curr. Res. Green Sustain. Chem.* **2021**, *4*, 100193. [CrossRef]
5. Overturf, E.; Ravasio, N.; Zaccheria, F.; Tonin, C.; Patrucco, A.; Bertini, F.; Canetti, M.; Avramidou, K.; Speranza, G.; Bavaro, T.; et al. Towards a more sustainable circular bioeconomy. Innovative approaches to rice residue valorization: The RiceRes case study. *Bioresour. Technol. Rep.* **2020**, *11*, 100427. [CrossRef]
6. Eksambekar, S. Silica Extracted from Rice Husk for Greener Tires, The Economist. Available online: https://www.economist.com/science-and-technology/2013/01/05/hysterectomy (accessed on 17 July 2024).
7. Solvay (2023, January 17). Solvay Launches Bio-Circular Silica in Europe, with Expansion Plans in North America. Available online: https://www.solvay.com/en/press-release/solvay-launches-bio-circular-silica-europe-expansion-plans-north-america (accessed on 17 July 2024).
8. Nguyen, T.T.; Ma, H.T.; Avti, P.; Bashir MJ, K.; Ng, C.A.; Wong, L.Y.; Jun, H.K.; Ngo, Q.M.; Tran, N.Q. Adsorptive Removal of Iron Using SiO_2 Nanoparticles Extracted from Rice Husk Ash. *J. Anal. Chem.* **2019**, *2019*, 6210240. [CrossRef] [PubMed]
9. Amirhandeh, S.Z.H.; Salem, A.; Salem, S. Treatment of tannery wastewater by silica nanoparticles produced from rice husk ash via a green route. Environmental science and pollution research international. *Environ. Sci. Pollut. Res. Int.* **2023**, *30*, 13039–13047. [CrossRef]
10. Porrang, S.; Rahemi, N.; Davaran, S.; Mahdavi, M.; Hassanzadeh, B. Preparation and in-vitro evaluation of mesoporous biogenic silica nanoparticles obtained from rice and wheat husk as a biocompatible carrier for anti-cancer drug delivery. *Eur. J. Pharm. Sci.* **2021**, *163*, 105866. [CrossRef]
11. Yalçin, N.; Sevinç, V. Studies on silica obtained from rice husk. *Ceram. Int.* **2021**, *27*, 219–224. [CrossRef]
12. Alyosef, H.A.; Eilert, A.; Welscher, J.; Ibrahim, S.S.; Denecke, R.; Schwieger, W.; Enke, D. Characterization of Biogenic Silica Generated by Thermo Chemical Treatment of Rice Husk. *Part. Sci. Technol.* **2013**, *31*, 524–532. [CrossRef]
13. Bakar, R.; Yahya, R.; Gan, S.N. Production of High Purity Amorphous Silica from Rice Husk. *Proc. Chem.* **2016**, *19*, 189–195. [CrossRef]
14. Chen, P.; Gu, W.; Fang, W.; Ji, X.; Bie, R. Removal of metal impurities in rice husk and characterization of rice husk ash under simplified acid pretreatment process. *Environ. Prog. Sustain.* **2017**, *36*, 830–837. [CrossRef]
15. Xu, W.; Wei, J.; Chen, J.; Zhang, B.; Xu, P.; Ren, J.; Yu, Q. Comparative Study of Water-Leaching and Acid-Leaching Pretreatment on the Thermal Stability and Reactivity of Biomass Silica for Viability as a Pozzolanic Additive in Cement. *Mater.* **2017**, *11*, 1697. [CrossRef] [PubMed]
16. Bakdash, R.S.; Aljundi, I.H.; Basheer, C.; Abdulazeez, I. Rice husk derived Aminated Silica for the efficient adsorption of different gases. *Sci. Rep.* **2020**, *10*, 19526. [CrossRef] [PubMed]
17. Russo, B.; Causse, J.; Rey, C.; Lautru, J.; Rebiscoul, D.; Ayral, A. Biosourced adsorbent prepared with rice husk part 1: A complete understanding of the structure of materials, the major role of mineral impurities for metal extraction. *Sustain. Mater. Techno.* **2023**, *36*, e00601. [CrossRef]
18. Sennoun, L.; Lee, C.C.; Fretel, Y.; Clavié, M.; Subra, G.; Ladner, Y.; Napoli, A.; Galarneau, A.; Hesemann, P.; Mehdi, A. Direct pseudomorphic transformation of silica from rice husk into organo-functionalized MCM-41. *New J. Chem.* **2024**, *48*, 7052–7069. [CrossRef]
19. Liou, T.-H.; Yang, C.-C. Synthesis and surface characteristics of nanosilica produced from alkali-extracted rice husk ash. *Mater. Sci. Eng. B* **2011**, *176*, 521–529. [CrossRef]
20. Gautam, N.; Rose, K.V.A.M.; Chaurasia, A.S. Study on chemical kinetics and characterization of nanosilica from rice husk and rice straw in the fixed-bed pyrolysis process. *Biomass Convers. Biorefinery* **2020**, *12*, 1435–1448. [CrossRef]
21. Su, Y.; Liu, L.; Zhang, S.; Xu, D.; Du, H.; Cheng, Y.; Wang, Z.; Xiong, Y. A green route for pyrolysis poly-generation of typical high ash biomass, rice husk: Effects on simultaneous production of carbonic oxide-rich syngas, phenol-abundant bio-oil, high-adsorption porous carbon and amorphous silicon dioxide. *Bioresour. Technol.* **2020**, *295*, 122243. [CrossRef]
22. Choudhary, P.; Sharma, R.; Kumar, V.; Singh, A.K.; Sharma, N. Synthesis, Characterization and Catalytic Activity of Bio-MCM-41 for Production of Bio Crude Oil via Pyrolysis of Rice Straw. *Waste Biomass Valori.* **2023**, *14*, 4173–4186. [CrossRef]
23. Gu, S.; Zhou, J.; Luo, Z.; Wang, Q.; Ni, M. A detailed study of the effects of pyrolysis temperature and feedstock particle size on the preparation of nanosilica from rice husk. *Ind. Crops Prod.* **2013**, *50*, 540–549. [CrossRef]
24. Gómez-Vásquez, R.; Fernández-Ballesteros, E.; Camargo-Trillos, D. Biogenic nanoporous oxides recovery from by-products of bioenergy production: Rice husks and corncob biochars. *Biomass Bioenergy* **2022**, *161*, 106455. [CrossRef]
25. Jyothsna, G.; Bahurudeen, A.; Sahu, P.K. Sustainable utilisation of rice husk for cleaner energy: A circular economy between agricultural, energy and construction sectors. *Mater. Today Sustain.* **2024**, *25*, 100667. [CrossRef]
26. Ahmaruzzaman, M.; Gupta, V.K. Rice Husk and Its Ash as Low-Cost Adsorbents in Water and Wastewater Treatment. *Ind. Eng. Chem. Res.* **2011**, *50*, 13589–13613. [CrossRef]

27. Ghosh, N.; Das, S.; Biswas, G.; Haldar, P.K. Review on some metal oxide nanoparticles as effective adsorbent in wastewater treatment. *Water Sci. Technol.* **2022**, *85*, 3370–3395. [CrossRef] [PubMed]
28. Rodriguez-Otero, A.; Vargas, V.; Galarneau, A.; Castillo, J.; Christensen, J.H.; Bouyssiere, B. Sustainable Harnessing of SiO_2 Nanoparticles from Rice Husks: A Review of the Best Synthesis and Applications. *Processes* **2023**, *11*, 3373. [CrossRef]
29. Saud, A.; Gupta, S.; Allal, A.; Preud'homme, H.; Shomar, B.; Zaidi, S.J. Progress in the Sustainable Development of Biobased (Nano)materials for Application in Water Treatment Technologies. *ACS Omega* **2024**, *9*, 29088–29113. [CrossRef]
30. Zarezadeh-Mehrizi, M.; Badiei, A. Highly efficient removal of basic blue 41 with nanoporous silica. *Water Resour. Ind.* **2014**, *5*, 49–57. [CrossRef]
31. Peres, E.C.; Slaviero, J.C.; Cunha, A.M.; Bandegharaei, A.H.; Dotto, G.L. Microwave synthesis of silica nanoparticles and its application for methylene blue adsorption. *J. Environ. Chem. Eng.* **2018**, *6*, 649–659. [CrossRef]
32. Tsamo, C.; Kidwang, G.D.; Dahaina, D.C. Removal of Rhodamine B from aqueous solution using silica extracted from rice husk. *SN Appl. Sci.* **2020**, *2*, 256. [CrossRef]
33. Grefa, D.D.A.; Sánchez, J.E.G.; Sánchez, L.R.B.; Alfonso, M.S.P.; Tagle, M.E.V. Rice husk ash as sorbent for solid phase extraction of diclofenac, ibuprofen and carboplatin residues from waters. *Microchem. J.* **2023**, *195*, 109361. [CrossRef]
34. Mondal MI, H.; Chakraborty, S.C.; Rahman, M.S.; Marjuban SM, H.; Ahmed, F.; Zhou, J.L.; Zargar, M. Adsorbents from rice husk and shrimp shell for effective removal of heavy metals and reactive dyes in water. *Environ. Pollut.* **2024**, *346*, 123637. [CrossRef]
35. Nandiyanto AB, D.; Nugraha, W.C.; Yustia, I.; Ragadhita, R.; Fiandini, M.; Meirinawati, H.; Wulan, D.R. Isotherm and kinetic adsorption of rice husk particles as a model adsorbent for solving issues in the sustainable gold mining environment from mercury leaching. *J. Min. Inst.* **2024**, *265*, 104–120.
36. Chander, S.; Yadav, S.; Gupta, A.; Luhach, N. Sequestration of Ni (II), Pb (II), and Zn (II) utilizing biogenic synthesized Fe3O4/CLPC NCs and modified Fe3O4/CLPC@CS NCs: Process optimization, simulation modeling, and feasibility study. *Environ. Sci. Pollut. Res.* **2023**, *30*, 114056–114077. [CrossRef] [PubMed]
37. Desmurs, L.; Galarneau, A.; Cammarano, C.; Hulea, V.; Vaulot, C.; Nouali, H.; Lebeau, B.; Daou, J.T.; Soares, C.V.; Maurin, G.; et al. Determination of Microporous and Mesoporous Surface Areas and Volumes of Mesoporous Zeolites by Corrected t-Plot Analysis. *Chem. Nano Mat.* **2022**, *8*, e202200051. [CrossRef]
38. Spitzmüller, L.; Nitschke, F.; Rudolph, B.; Berson, J.; Schimmel, T.; Kohl, T. Dissolution control and stability improvement of silica nanoparticles in aqueous media. *J. Nanoparticle Res.* **2023**, *25*, 40. [CrossRef]
39. Hu, S.; Jiang, L.; Wang, Y.; Su, S.; Sun, L.; Xu, B.; He, L.; Xiang, J. Effects of inherent alkali and alkaline earth metallic species on biomass pyrolysis at different temperatures. *Bioresour. Technol.* **2015**, *192*, 23–30. [CrossRef]
40. Zhang, S.; Zhu, S.; Zhang, H.; Chen, T.; Xiong, Y. Catalytic fast pyrolysis of rice husk: Effect of coupling leaching with torrefaction pretreatment. *J. Anal. Appl. Pyrolysis* **2018**, *133*, 91–96. [CrossRef]
41. Zhou, S.; Xue, Y.; Cai, J.; Cui, C.; Ni, Z.; Zhou, Z. An understanding for improved biomass pyrolysis: Toward a systematic comparison of different acid pretreatments. *Chem. Eng. J.* **2021**, *411*, 128513. [CrossRef]
42. Galarneau, A.; Calin, N.; Iapichella, J.; Barrande, M.; Denoyel, R.; Coasne, B.; Fajula, F. Optimization of the properties of macroporous chromatography silica supports through surface roughness control. *Chem Mater.* **2009**, *21*, 1884–1892. [CrossRef]
43. Agi, A.; Junin, R.; Gbadamosi, A.; Abbas, A.; Azli, N.B.; Oseh, J. Influence of nanoprecipitation on crystalline starch nanoparticle formed by ultrasonic assisted weak-acid hydrolysis of cassava starch and the rheology of their solutions. *Chem. Eng. Process.* **2019**, *142*, 107556. [CrossRef]
44. Schneider, M.; Cesca, K.; Maria, S.; Hotza, D.; Rodríguez-Castellón, E.; Moreira, R. Synthesis and characterization of silica-based nanofluids for enhanced oil recovery. *J. Mater. Res. Technol.* **2023**, *24*, 4143–4152. [CrossRef]
45. Musić, S.; Filipović-Vinceković, N.; Sekovanić, L. Precipitation of amorphous SiO_2 particles and their properties. *Braz. J. Chem. Eng.* **2011**, *28*, 89–94. [CrossRef]
46. Nayak, P.; Datta, A. Synthesis of SiO_2-Nanoparticles from Rice Husk Ash and its Comparison with Commercial Amorphous Silica through Material Characterization. *Silicon* **2021**, *13*, 1209–1214. [CrossRef]
47. Lal, M.; Sharma, P.; Ram, C. Synthesis and photocatalytic potential of Nd-doped TiO2 under UV and solar light irradiation using a sol-gel ultrasonication method. *Results Mater.* **2022**, *15*, 100308. [CrossRef]
48. Al-Saida, B.; Sandouqa, A.; Shawabkeh, R.A.; Hussein, I. Synthesis of Nanosilica for the Removal of Multicomponent Cd^{2+} and Cu^{2+} from Synthetic Water: An Experimental and Theoretical Study. *Molecules* **2022**, *27*, 7536. [CrossRef]
49. Gourmand, C.; Bertagnolli, C.; Brandel, J.; Hubscher-Bruder, V.; Boos, A. Bioinspired Mesoporous Silica for Cd(II) Removal from Aqueous Solutions. *Ind. Eng. Chem. Res.* **2022**, *61*, 8188–8203. [CrossRef]
50. Mehdinia, A.; Mehrabi, H.; Jabbari, A. Polythionine grafted onto magnetic SBA-15 for the removal of cadmium ions from aqueous solutions: Isothermal and kinetic studies. *New J. Chem.* **2019**, *43*, 5582–5591. [CrossRef]
51. Kamari, S.; Ghorbani, F. Synthesis of magMCM-41 with rice husk silica as cadmium sorbent from aqueous solutions: Parameters' optimization by response surface methodology. *Environ. Technol.* **2016**, *38*, 1562–1579. [CrossRef]
52. Simonescu, C.M.; Lavric, V.; Musina Antonescu, O.M.; Culita, D.C.; Marinescu, V.; Tardei, C.; Oprea, O.; Pandele, A.M. Experimental and modeling of cadmium ions removal by chelating resins. *J. Mol. Liq.* **2020**, *307*, 112973. [CrossRef]
53. Snoussi, Y.; Abderrabba, M.; Sayari, A. Removal of cadmium from aqueous solutions by adsorption onto polyethylenimine-functionalized mesocellular silica foam: Equilibrium properties. *J. Taiwan Inst. Chem. Eng.* **2016**, *66*, 372–378. [CrossRef]

54. Wang, P.; Shen, T.; Li, X.; Tang, Y.; Li, Y. Magnetic Mesoporous Calcium Carbonate-Based Nanocomposites for the Removal of Toxic Pb(II) and Cd(II) Ions from Water. *ACS App. Nano Mat.* **2020**, *3*, 1272–1281. [CrossRef]
55. Andooz, A.; Eqbalpour, M.; Kowsari, E.; Ramakrishna, S.; Cheshmeh, Z.A. A comprehensive review on pyrolysis from the circular economy point of view and its environmental and social effects. *J. Clean. Prod.* **2023**, *388*, 136021. [CrossRef]